CLINICAL GENETICS An International Journal of Genetics, Molecular and Personalized Medicine

Clin Genet 2013
Printed in Singapore. All rights reserved

CLINICAL GENETICS
doi: 10.1111/cge.12188

Letter to the Editor

AKT3 and *PIK3R2* mutations in two patients with megalencephaly-related syndromes: MCAP and MPPH

To the Editor:

Megalencephaly-capillary malformation syndrome (MCAP) and megalencephaly-polymicrogyria-polyd actyly-hydrocephalus syndrome (MPPH) belong to a spectrum of megalencephaly-related syndromes. The diagnostic criteria for MCAP include megalencephaly plus capillary malformations or syndactyly, and those for MPPH include megalencephaly and polymicrogyria, an absence of vascular anomalies, syndactyly, and brain heterotopia (1). Recently, *AKT3*, *PIK3R2*, and *PIK3CA* mutations have been identified in MCAP and MPPH (2). The proteins encoded by these genes are core components of the phosphatidylinositol 3-kinase (PI3K)-AKT pathway (3). Here, we report two patients with an *AKT3* and *PIK3R2* mutation. The study protocol was approved by the Institutional Review Boards for Ethical Issues at Yokohama City University and Yamagata University.

Patient 1 is an 8-year-old girl who has been previously reported as having MPPH (4). Brain magnetic resonance imaging (MRI) at 6 years showed asymmetry of the gyral pattern, dilated lateral ventricles, polymicrogyria, and abnormal signals in the occipital lobes, suggesting dysmyelination (Fig. 1a–c). Patient 2 is a 2-month-old boy who showed macrocephaly, cutis marmorata of the distal extremities, and hyperextensibility

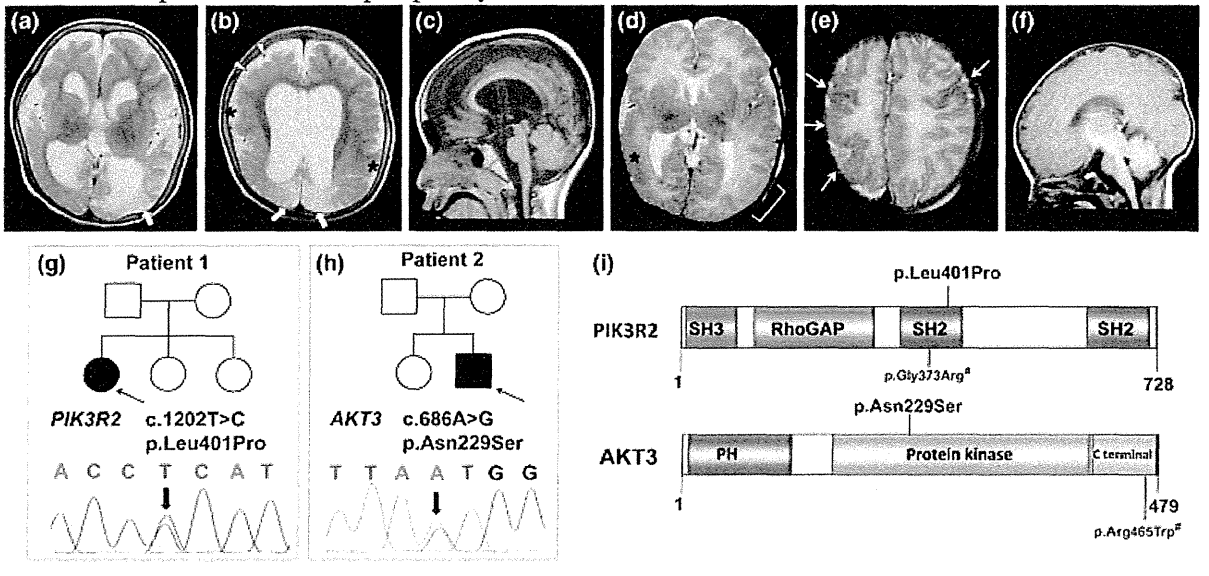

Fig. 1. Magnetic resonance imaging of patient 1 at 6 years of age (**a–c**). (**a, b**) Axial T2-weighted imaging showing enlarged lateral and third ventricles, enlarged extra-axial space, and decreased white matter volume with occipital lobe predominance. Irregular small gyri with areas of cortical thickening compatible with polymicrogyria are observed prominently in the bilateral perisylvian regions (asterisks) and the right frontal lobes (white arrowheads). Abnormal high-intensity signals are seen in the bilateral occipital lobes (thick white arrows). (c) Sagittal T1-weighted imaging showing normal brainstem and cerebellum. Magnetic resonance imaging of patient 2 at 7 days of age (**d–f**). (**d**) Axial T2-weighted imaging at the level of the basal ganglia showing enlargement of the left hemisphere. Polymicrogyria is seen in the perisylvian fissures with right-side dominance, which extends to the right temporal lobe (asterisk). The left parietal cortex shows a blurred border between the gray matter and the white matter (bracket), suggesting dysplasia of cortical development. (**e**) Axial T2-weighted imaging showing polymicrogyria in the right parietal lobe adjacent to the central sulcus (white arrows). (**f**) Sagittal T1-weighted imaging showing a relatively small pontine base. Family pedigrees and causative mutations (**g–i**). (g) Patient 1 with MPPH showing a *de novo* heterozygous missense mutation in *PIK3R2* (c.1202T>C, p.Leu401Pro). (h) Patient 2 with MCAP showing a *de novo* missense heterozygous mutation in *AKT3* (c.686A>G, p.Asn229Ser). (i) Distribution of mutations in *PIK3R2* and *AKT3*. SH2, Src homology 2 domain; SH3, Src homology 3 domain; RhoGAP, Rho GTPase-activating protein domain; PH, pleckstrin homology domain. #Reported by Riviere et al. (2).

of the skin. Brain MRI at 7 days showed an asymmetric cerebral hemisphere with right-dominant perisylvian polymicrogyria (Fig. 1d–f), and at 2 months showed a thin corpus callosum and progressive hydrocephalus. These findings were compatible with MCAP.

Whole exome sequencing using DNA extracted from blood leukocytes revealed a *de novo* missense mutation in each patient: p.Leu401Pro in *PIK3R2* (patient 1) and p.Asn229Ser in *AKT3* (patient 2) (Fig. 1g–i). Both mutations were absent from the 6500 eomes sequenced by the National Heart, Lung, and Blood Institute exome project and our 144 in-house control exomes. The read count for mutant alleles possessing p.Leu401Pro in *PIK3R2* was 47.7% (84/176 reads), and that for p.Asn229Ser in *AKT3* was 52.2% (128/245 reads). Therefore, these mutations are likely germline rather than mosaic mutations.

The novel *PIK3R2* mutation (p.Leu401Pro) in patient 1 is within the first Src homology 2 (SH2) domain of the PIK3R2 protein; this domain binds to phosphotyrosine-containing motifs and regulates many aspects of cellular communication (5). Eleven MPPH families have been reported to have a recurrent *PIK3R2* mutation (p.Gly373Arg), which is also located in the first SH2 domain (2). The phenotypes of all 13 cases with the p.Gly373Arg mutation were similar to that of patient 1 (Table 1) (1, 2), implying that impaired function of the SH2 domain is important in the pathogenesis of MPPH. The *AKT3* mutation (p.Asn229Ser) detected in patient 2 with MCAP has been reported in a case of MPPH (2). Furthermore, another case with a different *AKT3* mutation (p.Arg465Trp) was diagnosed with overlapping features of MCAP and MPPH (Table 1). These findings support the notion that the two syndromes have a common genetic basis. Interestingly, somatic mosaicism of an *AKT3* mutation causes hemimegalencephaly, which is similar to MPPH or MCAP (6, 7). Mutation screening of *AKT3* should be considered for patients with MPPH or MCAP as well as those with hemimegalencephaly, for whom pathological tissue is available.

MCAP and MPPH are categorized as overgrowth syndromes, as are Cowden disease and Proteus syndrome that are caused by abnormal activation of the PI3K–AKT pathway, which participates in diverse cellular processes (3, 8). The PI3K–AKT pathway is linked to mammalian target of rapamycin (mTOR) (6), which is a specific molecule for targeted therapeutics (sirolimus or everolimus). Further investigation into potential treatments for overgrowth syndromes is essential.

In summary, we have described two patients with either an *AKT3* or a *PIK3R2* mutation. Our data highlight the importance of the SH2 domain of PIK3R2 in MPPH, and support that MPPH and MCAP have the same genetic origin.

Table 1. Phenotypes associated with *PIK3R2* and *AKT3* mutations

Patient (diagnosis)	Patient 1 (MPPH)	13 patients[a] (MPPH)	Patient 2 (MCAP)	LR11-354[a] (MPPH)	LR08-018[a] (overlapping MCAP and MPPH)
Mutation	*PIK3R2* (p.Leu401Pro)	*PIK3R2* (p.Gly373Arg)	*AKT3* (p.Asn229Ser)	*AKT3* (p.Asn229Ser)	*AKT3* (p.Arg465Trp)
Features					
HC SD (age)	+2.6 (1 y 9 m)	+2–8 (8 m–13 y)	+3.0 (2 m)	+6.0 (2 y 5 m)	+5.5 (7.5 m)
Overgrowth	–	2/13	–	–	–
Vascular abnormalities	–	0/13	Skin capillary malformation	–	umbilical hemangioma
Connective tissue dysplasia	–	0/13	+	+	+
Syndactyly	–	0/13	–	–	–
Polydactyly	+	2/13	–	–	–
Epileptic seizures	+	6/9	+	ND	+
Visual impairment	+	ND	–	ND	ND
Neuroimaging features					
Polymicrogyria	+	13/13	+	+	+
Hydrocephalus or ventriculomegaly	+	13/13	+	+	+
CBTE	–	8/13	–	–	+

MPPH, megalencephaly-polymicrogyria-polydactyly-hydrocephalus syndrome; MCAP, megalencephaly-capillary malformation syndrome; HC, head circumference; SD, standard deviation; y, years; m, months; ND, no data; CBTE, cerebellar tonsillar ectopia.
[a] Riviere et al. (2) and Mirzaa et al. (1).

Acknowledgements

We would like to thank the patients and their families for their participation in this study. We thank Aya Narita for technical

assistance. This work was supported by the Ministry of Health, Labour, and Welfare of Japan (24133701,11103577, 11103340 and 10103235); a Grant-in-Aid for Scientific Research (C) from the Japan Society for the Promotion of Science (24591500); a Grant-in-Aid for Young Scientists from the Japan Society for the Promotion of Science (10013428 and 12020465); the Takeda Science Foundation; the Japan Science and Technology Agency; the Strategic Research Program for Brain Sciences (11105137); and a Grant-in-Aid for Scientific Research on Innovative Areas (Transcription Cycle) from the Ministry of Education, Culture, Sports, Science, and Technology of Japan (12024421).

K Nakamura[a,b]
M Kato[b]
J Tohyama[c]
T Shiohama[d]
K Hayasaka[b]
K Nishiyama[a]
H Kodera[a]
M Nakashima[a]
Y Tsurusaki[a]
N Miyake[a]
N Matsumoto[a]
H Saitsu[a]
[a]Department of Human Genetics
Yokohama City University Graduate School of Medicine
Yokohama, Japan
[b]Department of Pediatrics
Yamagata University Faculty of Medicine
Yamagata, Japan
[c]Department of Pediatrics
Epilepsy Center, Nishi-Niigata Chuo National Hospital
Niigata, Japan
[d]Department of Pediatrics
Kimitsu Chuo Hospital
Chiba, Japan

References

1. Mirzaa GM, Conway RL, Gripp KW et al. Megalencephaly-capillary malformation (MCAP) and megalencephaly-polydactyly-poly microgyria-hydrocephalus (MPPH) syndromes: two closely related disorders of brain overgrowth and abnormal brain and body morphogenesis. Am J Med Genet A 2012: 158A: 269–291.
2. Riviere JB, Mirzaa GM, O'Roak BJ et al. De novo germline and postzygotic mutations in *AKT3*, *PIK3R2* and *PIK3CA* cause a spectrum of related megalencephaly syndromes. Nat Genet 2012: 44: 934–940.
3. Franke TF. PI3K/Akt: getting it right matters. Oncogene 2008: 27: 6473–6488.
4. Tohyama J, Akasaka N, Saito N, Yoshimura J, Nishiyama K, Kato M. Megalencephaly and polymicrogyria with polydactyly syndrome. Pediatr Neurol 2007: 37: 148–151.
5. Liu BA, Jablonowski K, Raina M, Arcé M, Pawson T, Nash PD. The human and mouse complement of SH2 domain proteins – establishing the boundaries of phosphotyrosine signaling. Mol Cell 2006: 22: 851–868.
6. Lee JH, Huynh M, Silhavy JL et al. De novo somatic mutations in components of the PI3K-AKT3-mTOR pathway cause hemimegalencephaly. Nat Genet 2012: 44: 941–945.
7. Poduri A, Evrony GD, Cai X et al. Somatic activation of AKT3 causes hemispheric developmental brain malformations. Neuron 2012: 74: 41–48.
8. Lindhurst MJ, Sapp JC, Teer JK et al. A mosaic activating mutation in *AKT1* associated with the Proteus syndrome. N Engl J Med 2011: 365: 611–619.

Correspondence:
Dr Kazuyuki Nakamura, MD
Department of Pediatrics
Yamagata University Faculty of Medicine
2-2-2 Iida-nishi
Yamagata 990-9585
Japan
Tel: +81-23-628-5329
Fax: +81-23-628-5331
e-mail: kazun-yamagata@umin.ac.jp

RESEARCH ARTICLE

AMERICAN JOURNAL OF medical genetics PART A

Whole-Exome Sequencing Identified a Homozygous *FNBP4* Mutation in a Family With a Condition Similar to Microphthalmia with Limb Anomalies

Yukiko Kondo,[1] Eriko Koshimizu,[1] Andre Megarbane,[2] Haruka Hamanoue,[3] Ippei Okada,[1] Kiyomi Nishiyama,[1] Hirofumi Kodera,[1] Satoko Miyatake,[1] Yoshinori Tsurusaki,[1] Mitsuko Nakashima,[1] Hiroshi Doi,[1] Noriko Miyake,[1] Hirotomo Saitsu,[1] and Naomichi Matsumoto[1]*

[1]Department of Human Genetics, Yokohama City University Graduate School of Medicine, Kanazawa-ku, Yokohama, Japan

[2]Medecal Genetics Unit, St. Joseph University, Beirut, Lebanon

[3]Department of Obstetrics and Gynecology, Yokohama City University Graduate School of Medicine, Kanazawa-ku, Yokohama, Japan

Manuscript Received: 4 January 2013; Manuscript Accepted: 9 March 2013

Microphthalmia with limb anomalies (MLA), also known as Waardenburg anophthalmia syndrome or ophthalmoacromelic syndrome, is a rare autosomal recessive disorder. Recently, we and others successfully identified *SMOC1* as the causative gene for MLA. However, there are several MLA families without *SMOC1* abnormality, suggesting locus heterogeneity in MLA. We aimed to identify a pathogenic mutation in one Lebanese family having an MLA-like condition without *SMOC1* mutation by whole-exome sequencing (WES) combined with homozygosity mapping. A c.683C>T (p.Thr228Met) in *FNBP4* was found as a primary candidate, drawing the attention that FNBP4 and SMOC1 may potentially modulate BMP signaling. © 2013 Wiley Periodicals, Inc.

Key words: microphthalmia with limb anomaly; homozygous mutation; *FNBP4*; *SMOC1*; whole-exome sequencing (WES)

How to Cite this Article:
Kondo Y, Koshimizu E, Megarbane A, Hamanoue H, Okada I, Nishiyama K., Kodera H., Miyatake S, Tsurusaki Y, Nakashima M, Doi H, Miyake N, Saitsu H, Matsumoto N. 2013. Whole-exome sequencing identified a homozygous *FNBP4* mutation in a family with a condition similar to microphthalmia with limb anomalies.
Am J Med Genet Part A 161A:1543–1546.

INTRODUCTION

Microphthalmia with limb anomalies (MLA [OMIM #206920]), also known as Waardenburg anophthalmia syndrome or ophthalmoacromelic syndrome, is a rare autosomal recessive disorder first described by Waardenburg in 1935. Approximately 90% of families with MLA patients are consanguineous [Garavelli et al., 2006]. In 2011, 25 families were clinically reviewed [Rainger et al., 2011]. Patients show anophthalmia (91.4%, mostly bilateral), lower limb postaxial oligodactyly (82.9%), syndactyly of metacarpals 4th–5th finger (57.1%), and learning disability (37.1%) [Rainger et al., 2011]. We and others successfully identified *SMOC1* causative for MLA [Abouzeid et al., 2011; Okada et al., 2011]. Of note, seven of 18 families did not show *SMOC1* abnormalities [Okada et al., 2011; Rainger et al., 2011], indicating the locus heterogeneity in MLA. In this report, we present the result of whole-exome sequencing (WES) in one *SMOC1*-negative family with a condition like MLA.

CLINICAL REPORT

The Lebanese family with a condition like MLA was previously described in detail (Fig. 1A) [Megarbane et al., 1998; Hamanoue et al., 2009; Okada et al., 2011]. Briefly, the main clinical features affecting the patient (anophthalmia, syndactyly of 2nd–3rd fingers on the right hand, postaxial polydactyly on the right foot, and

Additional supporting information may be found in the online version of this article.

Grant sponsor: Ministry of Health, Labor and Welfare of Japan; Grant sponsor: Japan Society for the Promotion of Science; Grant sponsor: Japan Science and Technology Agency; Grant sponsor: Ministry of Education, Culture, Sports, Science and Technology; Grant sponsor: Takeda Science Foundation.

*Correspondence to:
Dr. Naomichi Matsumoto, Department of Human Genetics, Yokohama City University Graduate School of Medicine, Fukuura 3-9, Kanazawa-ku, Yokohama 236-0004, Japan. E-mail: naomat@yokohama-cu.ac.jp

Article first published online in Wiley Online Library (wileyonlinelibrary.com): 23 May 2013
DOI 10.1002/ajmg.a.35983

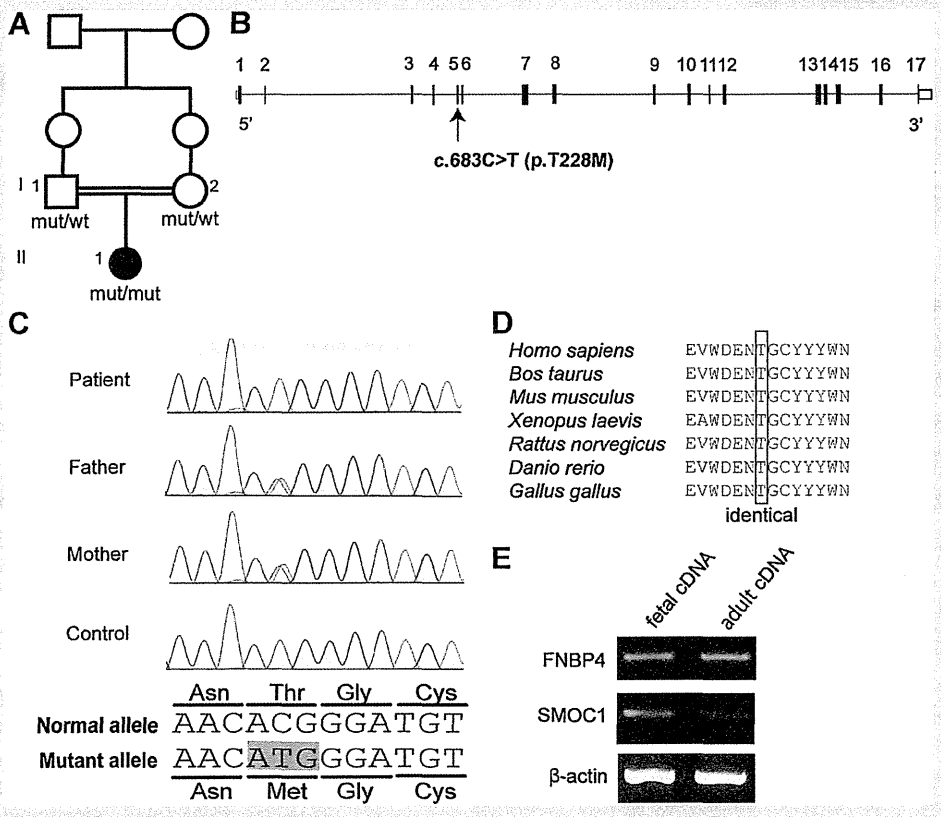

FIG. 1. Pedigree and *FNBP4* mutation and expression. A: Pedigree of the consanguineous MLA family. Black and open symbols denote affected and unaffected individuals, respectively. mut, mutant allele; wt, wild-type allele (B) Schematic representation of the *FNBP4*. UTR and coding region are open and filled rectangles, respectively. The location of the c.683C>T mutation is indicated by arrow. C: Electropherograms of the patient with a homozygous mutation (top), unaffected parents with a heterozygous mutation (middle) and a control with no mutation (bottom). A single nucleotide alteration in exon 5 caused an amino acid alteration. D: The missense mutation occurred at the evolutionally conserved amino acids. Homologous sequences were aligned using the CLUSTALW website (http://align.genome.jp/). E: Expression analysis by PCR using human fetal and adult eye cDNA. *FNBP4*, *SMOC1* and β-actin were amplified.

bilateral ectrodactyly of the upper limbs) are somehow different from those of the classic MLA caused by *SMOC1* mutation (anophthalmia and limb anomalies such as postaxial oligosyndactyly).

GENETIC STUDIES

Genomic DNA was obtained from peripheral blood leukocytes using QuickGene 610-L (Fujifilm, Tokyo, Japan) after informed consent was given. DNA was amplified using GenomiPhi V2 kit (GE healthcare, Buckinghamshire, UK). Experimental protocols were approved by the Institutional Review Board of Yokohama City University School of Medicine. Seven anophthalmia-related genes (eTable SI—see Supporting Information online) were negative by Sanger sequencing. To check copy number variations (CNVs), the Genome-wide Human SNP Array 6.0 (Affymetrix, Santa Clara, CA) with Genotyping Console 3.0.1 (Copy Number Analyzer for GeneChip; Affymetrix) was used according to the manufacturer's instructions. No pathological CNVs were detected in the patient. Then, the SNP Array 6.0 data was also used for homozygosity mapping with HomozygosityMapper software [Bahlo and Bromhead, 2009]. A total of 14 >1-Mb homozygous regions were revealed, amounting to approximately 118.4 Mb in size and including 625 genes (eTable SII—see Supporting Information online). Among them, 14 candidate genes were negative by Sanger sequencing (eTable SI—see Supporting Information online).

WES was then performed. Three micrograms of DNA from the patient and his parents were processed using the SureSelect Human All Exon 50 Mb Kit (Agilent Technologies, Santa Clara, CA) or the SureSelect Human All Exon Kit v4 (51 Mb; Agilent) to generate exome libraries. The libraries were sequenced with an Illumina GAIIx (Illumina Inc, San Diego, CA) or an Illumina Hiseq2000 (Illumina) with paired-end reads, according to the manufacturer's instructions. Image analysis and base calling were performed by Sequence Control Software with Real-Time Analysis (Illumina) and

CASAVA software v1.7 (Illumina). Reads from GAIIx and Hiseq2000 were aligned and mapped to the human reference genome sequence (UCSC Genome Browser hg19, NCBI genome sequence website build 37) using Novoalign (Novocraft, Selangor, Malaysia; http://www.novocraft.com/main/index.php). Variant call as well as coverage and depth calculations were performed using the Genome Analysis Toolkit. Called single nucleotide variants (SNVs) were annotated with Annovar (Center for Applied Genomics, Children's Hospital of Philadelphia, Philadelphia, USA). Candidate variants were confirmed by Sanger sequencing with a 3130xL or 3500xL Genetic Analyzer (Applied Biosystems, Foster City, CA). The Human Gene Mutation Database (Biobases, Wolfenbuettel, Germany; https://portal.biobase-international.com/hgmd/pro/start.php) was used for checking whether the variants had been previously reported. PolyPhen-2 (http://genetics.bwh.harvard.edu/pph2/), SIFT (http://sift.jcvi.org/www/SIFT_BLink_submit.html), and MutationTaster (http://www.mutationtaster.org/) were used to evaluate variants in terms of sequence conservation, chemical change, and likelihood of pathogenicity. More than 85% of target regions were covered by 10 reads or more (eTable SIII—see Supporting Information online).

We adopted the following prioritization scheme to narrow down pathogenic mutations (Table I). First, we excluded the variants registered in the dbSNP135. In the trio (patient and parents) analysis, 844 SNVs of non-synonymous, canonical splice site change or small insertions or deletions were identified. Variants in segmental duplications or repeat elements registered in the Database of Genomic Variants (http://projects.tcag.ac/variation/) were excluded. Homozygous or compound heterozygous variants were picked up and confirmed by Sanger sequencing. Finally, five homozygous mutations and four heterozygous mutations remained, which were completely co-segregated with MLA (Table I). These variants were not found in the National Heart, Lung, and Blood Institute Exome Sequencing Project Exome Variant Server (5,400 exomes; http://evs.gs.washington.edu/EVS/), or our in-house 170 exomes. Among these, the homozygous mutation [c.683C>T (p.Thr228Met)] in *FNBP4* (NM_015308) is the primary candidate (Fig. 1A–C). The mutation occurred at the evolutionarily conserved amino acid among different species (Fig. 1D). PolyPhen-2, SIFT, and MutationTaster indicate "probably damaging," "pathogenic," and "disease causing," respectively. All the other homozygous and compound heterozygous variants were unlikely pathogenic based on the web-based analyses (eTable SI—see Supporting Information online).

Substantial *FNBP4* expression in eye tissues was confirmed by PCR using complementary DNA (cDNA) from human fetal and adult eye tissues (Biochain, Newark, CA; Fig. 1E). PCR mixture containing 2.5-ng cDNA, 1× ExTaq buffer, 2.5 mM each dNTP, 0.5 M each primer, and 0.25 U ExTaq HS polymerase (TakaraBio, Ohtsu, Japan) were cycled 35 times at 94°C for 30 sec, 60°C for 30 sec, and 72°C for 30 sec. β-Actin and *SMOC1* (NM_001034852) were checked as positive controls. Primer information is available on request.

Knockdown experiments using zebrafish showed unexplained uniform early lethality with eye malformations which hamper appropriate evaluation partly due to small sizes (Supplemental eFig. 1—see Supporting Information online).

DISCUSSION

FNBP4 encodes formin binding protein 4 which interacts with FH1 domains in Formin1 (FMN1). Formin family proteins play as key regulators of actin and microtubule cytoskeletal dynamics during cell division and migration [Frazier and Field, 1997; Wasserman, 1998], but FNBP4 function remains undetermined. This patient presents with ectrodactyly, which is exceptional in MLA. For normal limb development, three cell clusters including the apical ectodermal ridge (AER), the progress zone (PZ), and the zone of polarizing activity (ZPA) are of primary importance and produce signaling molecules determining the fate of neighboring cells by instructing them to remain undifferentiated, to proliferate, or to differentiate [Duijf et al., 2003]. Ectrodactyly is caused by error in the initiation and maintenance of the AER in the developing limb bud and disruption in signaling between the ZPA and the AER [Robledo et al., 2002]. Signals from the AER, including fibroblast growth factors, bone morphogenetic proteins (BMPs) and WNT signaling, allow the underlying mesenchymal cells of the PZ to maintain their proliferative activity, being modulated by Sonic

TABLE I. Sequence Variants Identified by Whole-Exome Sequencing

	Patient–parents trio
	Novoalign/GATK/Annovar
Total variant calls (not in dbSNP135)	1,414
Variants not located in segmental duplications	1,115
NS + SP + indels	844
Candidate variants (AR model) (homozygous/compound heterozygous)	38/366
Segregation confirmed genes (homozygous/compound heterozygous)	13/28
Variants not found in 170 in-house exomes (homozygous/compound heterozygous)	5/4
Predicted candidate genes to be pathogenic (homozygous/compound heterozygous)	1/0 *FNBP4*: c.683C>T (p.Thr228Met)

GATK, Genome Analysis Toolkit; SNP, single nucleotide polymorphism; NS, non-synonymous variants; SP, canonical splice site variants; indels, small insertions or deletions. AR, autosomal recessive inheritance; SIFT, PolyPhen-2 and MutationTaster were used to predict the impact of an amino acid substitution on the structure and function of a human protein.

Hedgehog signaling from the ZPA, through FMN1 and Gremlin [Duijf et al., 2003]. FMN1, which represses BMP signaling in association with cytoskeleton components, has previously been implicated in limb development [Zhou et al., 2009]. SMOC1 also functions as a BMP antagonist in early embryogenesis, which provides a plausible explanation for both the limb and eye phenotype in humans and mice [Okada et al., 2011; Rainger et al., 2011].

In conclusion, *FNBP4* is mutated in a Lebanese family with MLA. This knowledge is useful to understand development of eye and limb in humans.

ACKNOWLEDGMENTS

We would like to thank the patients and their families for their participation in this study. This work was supported by the Ministry of Health, Labor and Welfare of Japan, a Grant-in-Aid from the Japan Society for the Promotion of Science, a Grant-in-Aid for Young Scientists from the Japan Society for the Promotion of Science, the Japan Science and Technology Agency, the Strategic Research Program for Brain Sciences, a Grant-in-Aid for Scientific Research on Innovative Areas (Transcription Cycle) from the Ministry of Education, Culture, Sports, Science and Technology of Japan and Takeda Science Foundation.

REFERENCES

Abouzeid H, Boisset G, Favez T, Youssef M, Marzouk I, Shakankiry N, Bayoumi N, Descombes P, Agosti C, Munier FL, Schorderet DF. 2011. Mutations in the SPARC-related modular calcium-binding protein 1 gene, SMOC1, cause waardenburg anophthalmia syndrome. Am J Hum Genet 88:92–98.

Bahlo M, Bromhead CJ. 2009. Generating linkage mapping files from Affymetrix SNP chip data. Bioinformatics 25:1961–1962.

Duijf PH, van Bokhoven H, Brunner HG. 2003. Pathogenesis of split-hand/split-foot malformation. Hum Mol Genet 12:R51–R60.

Frazier JA, Field CM. 1997. Actin cytoskeleton: Are FH proteins local organizers? Curr Biol 7:R414–R417.

Garavelli L, Pedori S, Dal Zotto R, Franchi F, Marinelli M, Croci GF, Bellato S, Ammenti A, Virdis R, Banchini G, Superti-Furga A. 2006. Anophthalmos with limb anomalies (Waardenburg opththalmo (sic)-acromelic syndrome): report of a new Italian case with renal anomaly and review. Genet Couns 17:449–455.

Hamanoue H, Megarbane A, Tohma T, Nishimura A, Mizuguchi T, Saitsu H, Sakai H, Miura S, Toda T, Miyake N, Niikawa N, Yoshiura K, Hirahara F, Matsumoto N. 2009. A locus for ophthalmo-acromelic syndrome mapped to 10p11. 23. Am J Med Genet Part A 149A:336–342.

Megarbane A, Souraty N, Tamraz J. 1998. Ophthalmo-acromelic syndrome (Waardenburg) with split hand and polydactyly. Genet Couns 9:195–199.

Okada I, Hamanoue H, Terada K, Tohma T, Megarbane A, Chouery E, Abou-Ghoch J, Jalkh N, Cogulu O, Ozkinay F, Horie K, Takeda J, Furuichi T, Ikegawa S, Nishiyama K, Miyatake S, Nishimura A, Mizuguchi T, Niikawa N, Hirahara F, Kaname T, Yoshiura K, Tsurusaki Y, Doi H, Miyake N, Furukawa T, Matsumoto N, Saitsu H. 2011. SMOC1 is essential for ocular and limb development in humans and mice. Am J Hum Genet 88:30–41.

Rainger J, van Beusekom E, Ramsay JK, McKie L, Al-Gazali L, Pallotta R, Saponari A, Branney P, Fisher M, Morrison H, Bicknell L, Gautier P, Perry P, Sokhi K, Sexton D, Bardakjian TM, Schneider AS, Elcioglu N, Ozkinay F, Koenig R, Megarbane A, Semerci CN, Khan A, Zafar S, Hennekam R, Sousa SB, Ramos L, Garavelli L, Furga AS, Wischmeijer A, Jackson IJ, Gillessen-Kaesbach G, Brunner HG, Wieczorek D, van Bokhoven H, Fitzpatrick DR. 2011. Loss of the BMP antagonist, SMOC-1, causes Ophthalmo-acromelic (Waardenburg Anophthalmia) syndrome in humans and mice. PLoS Genet 7:e1002114.

Robledo RF, Rajan L, Li X, Lufkin T. 2002. The Dlx5 and Dlx6 homeobox genes are essential for craniofacial, axial, and appendicular skeletal development. Genes Dev 16:1089–1101.

Wasserman S. 1998. FH proteins as cytoskeletal organizers. Trends Cell Biol 8:111–115.

Zhou F, Leder P, Zuniga A, Dettenhofer M. 2009. Formin1 disruption confers oligodactylism and alters Bmp signaling. Hum Mol Genet 18:2472–2482.

Mutations in *B3GALT6*, which Encodes a Glycosaminoglycan Linker Region Enzyme, Cause a Spectrum of Skeletal and Connective Tissue Disorders

Masahiro Nakajima,[1,21] Shuji Mizumoto,[2,21] Noriko Miyake,[3,21] Ryo Kogawa,[2] Aritoshi Iida,[1] Hironori Ito,[4] Hiroshi Kitoh,[5] Aya Hirayama,[6] Hiroshi Mitsubuchi,[7] Osamu Miyazaki,[8] Rika Kosaki,[9] Reiko Horikawa,[10] Angeline Lai,[11] Roberto Mendoza-Londono,[12] Lucie Dupuis,[12] David Chitayat,[12] Andrew Howard,[13] Gabriela F. Leal,[14] Denise Cavalcanti,[15] Yoshinori Tsurusaki,[3] Hirotomo Saitsu,[3] Shigehiko Watanabe,[16] Ekkehart Lausch,[17] Sheila Unger,[18] Luisa Bonafé,[19] Hirofumi Ohashi,[16] Andrea Superti-Furga,[19] Naomichi Matsumoto,[3] Kazuyuki Sugahara,[2] Gen Nishimura,[20] and Shiro Ikegawa[1,*]

Proteoglycans (PGs) are a major component of the extracellular matrix in many tissues and function as structural and regulatory molecules. PGs are composed of core proteins and glycosaminoglycan (GAG) side chains. The biosynthesis of GAGs starts with the linker region that consists of four sugar residues and is followed by repeating disaccharide units. By exome sequencing, we found that *B3GALT6* encoding an enzyme involved in the biosynthesis of the GAG linker region is responsible for a severe skeletal dysplasia, spondyloepimetaphyseal dysplasia with joint laxity type 1 (SEMD-JL1). *B3GALT6* loss-of-function mutations were found in individuals with SEMD-JL1 from seven families. In a subsequent candidate gene study based on the phenotypic similarity, we found that *B3GALT6* is also responsible for a connective tissue disease, Ehlers-Danlos syndrome (progeroid form). Recessive loss-of-function mutations in *B3GALT6* result in a spectrum of disorders affecting a broad range of skeletal and connective tissues characterized by lax skin, muscle hypotonia, joint dislocation, and spinal deformity. The pleiotropic phenotypes of the disorders indicate that *B3GALT6* plays a critical role in a wide range of biological processes in various tissues, including skin, bone, cartilage, tendon, and ligament.

Skeletal dysplasias represent a vast collection of genetic disorders of the skeleton, currently divided into 40 groups.[1] Spondyloepimetaphyseal dysplasia (SEMD) is one group (group 13) of skeletal dysplasia that contains more than a dozen distinctive diseases. SEMD with joint laxity (SEMD-JL) is a subgroup of SEMD that consists of type 1 (SEMD-JL1 [MIM 271640]) and type 2 (SEMD-JL2 [MIM 603546]). SEMD-JL1 or SEMD-JL Beighton type is an autosomal-recessive disorder that shows mild craniofacial dysmorphism (prominent eye, blue sclera, long upper lip, small mandible with cleft palate) and spatulate finger with short nail.[2] The large joints of individuals with SEMD-JL1 are variably affected with hip dislocation, elbow contracture secondary to radial head dislocation, and clubfeet. Joint laxity is particularly prominent in the hands. Skeletal changes of SEMD-JL1 are characterized by moderate platyspondyly with anterior projection of the vertebral bodies, hypoplastic ilia, and mild metaphyseal flaring.[3] Kyphoscoliosis progresses with age, leading to a short trunk, whereas platyspondyly become less conspicuous and the vertebral bodies appear squared in shape with age. Recently, dominant kinesin family member 22 (*KIF22* [MIM 603213]) mutations have been found in SEMD-JL2;[4,5] however, the genetic basis of SEMD-JL1 remains unknown.

To identify the SEMD-JL1-causing mutation, we performed whole-exome sequencing experiments. We recruited seven individuals with SEMD-JL1 from five unrelated Japanese families (F1–F5) and a Singapore/Japanese family (F6) (Table 1). One family (F1) had a pair of affected sibs (P1 and P2) from nonconsanguineous parents. Genomic DNA was extracted by standard procedures

[1]Laboratory for Bone and Joint Diseases, Center for Integrative Medical Sciences, RIKEN, Tokyo 108-8639, Japan; [2]Laboratory of Proteoglycan Signaling and Therapeutics, Frontier Research Center for Post-Genomic Science and Technology, Graduate School of Life Science, Hokkaido University, Sapporo 001-0021, Japan; [3]Department of Human Genetics, Yokohama City University Graduate School of Medicine, Yokohama 236-0004, Japan; [4]Department of Orthopaedic Surgery, Central Hospital, Aichi Prefectural Colony, Kasugai 480-0392, Japan; [5]Department of Orthopaedic Surgery, Nagoya University School of Medicine, Nagoya 466-8550, Japan; [6]Department of Pediatrics, Akita Prefectural Center on Development and Disability, Akita 010-1407, Japan; [7]Department of Neonatology, Kumamoto University Hospital, Kumamoto 860-8556, Japan; [8]Department of Radiology, National Center for Child Health and Development, Tokyo 157-8535, Japan; [9]Division of Medical Genetics, National Center for Child Health and Development, Tokyo 157-8535, Japan; [10]Division of Endocrinology and Metabolism, National Center for Child Health and Development, Tokyo 157-8535, Japan; [11]Department of Paediatric Medicine, KK Women's and Children's Hospital, Singapore 229899, Singapore; [12]Department of Paediatrics, The Hospital for Sick Children and University of Toronto, Toronto, ON M5G 1X8, Canada; [13]Department of Surgery, The Hospital for Sick Children and University of Toronto, Toronto, ON M5G 1X8, Canada; [14]The Professor Fernando Figueira Integral Medicine Institute (IMIP), Recife, PE 50070-550, Brazil; [15]Skeletal Dysplasia Group, Department of Medical Genetics, Faculty of Medical Sciences, State University of Campinas (UNICAMP), Campinas, SP 13083-970, Brazil; [16]Division of Medical Genetics, Saitama Children's Medical Center, Saitama 339-8551, Japan; [17]Division of Paediatric Genetics, Centre for Pediatrics and Adolescent Medicine, University of Freiburg, Freiburg 79106, Germany; [18]Medical Genetics Service, University of Lausanne, CHUV, Lausanne 1011, Switzerland; [19]Department of Pediatrics, University of Lausanne, CHUV, Lausanne 1011, Switzerland; [20]Department of Pediatric Imaging, Tokyo Metropolitan Children's Medical Center, Fuchu 183-8561, Japan
[21]These authors contributed equally to this work
*Correspondence: sikegawa@ims.u-tokyo.ac.jp
http://dx.doi.org/10.1016/j.ajhg.2013.04.003.

Table 1. Clinical and Radiographic Findings of the Individuals with *B3GALT6* Mutations

Subject ID	P1	P2	P3	P4	P5	P6	P7	P8	P9	P10	P11	P12
Family ID	F1	F1	F2	F3	F4	F5	F6	F7	F8	F9	F9	F10
Clinical diagnosis	SEMD-JL1	SEMD-JL1	SEMD-JL1	SEMD-JL1	SEMD-JL1	SEMD-JL1	SEMD-JL1	SEMD-JL1	EDS-PF	EDS-PF	EDS-PF	EDS-PF
General Information												
Ethnicity	Japanese	Japanese	Japanese	Japanese	Japanese	Japanese	Japanese/ Singaporean	Vietnamese	Italian	Italian/ Canadian	Italian/ Canadian	Brazilian
Gender	M	M	F	M	F	F	M	M	M	F	F	F
Age	34 years	31 years	12 years, 7 months	6 years	5 years, 1 month	12 years	2 years, 9 months	34 years	8 months	7 years	1 month	5 years, 1 month
Gestational age	39 weeks, 2 days	full term	37 weeks	40 weeks, 1 day	39 weeks, 5 days	full term	39 weeks	full term	ND	36 weeks	37 weeks	39 weeks
Birth length (cm)	ND	ND	36	ND	43.1	42	43	(average)	ND	44	44	44
Birth weight (g)	ND	2,200	2,124	2,832	2,535	2,222	2,485	3,500	ND	2,097	2,790	3,300
Clinical Features												
Height (cm) (SD)[a]	127.7 (−7.4)	130 (−7.0)	88.8 (−10.7)	94 (−4.0)	90 (−4.0)	118.4 (−5.1)	78.2 (−4.0)	118 (−9.1)	66 (−1.6)	90 (−6.8)	45 (−3.7)	81 (−5.9)
Weight (kg) (SD)[a]	40.3 (−2.2)	36.9 (−2.5)	13.2 (−3.7)	15.4 (−1.5)	14.4 (−1.3)	23.2 (−2.0)	10.6 (−1.9)	28 (−3.3)	5.65 (−3.0)	13.9 (−2.2)	2.65 (−2.8)	8.5 (−8.4)
Craniofacial												
Flat face with prominent forehead	ND	ND	+	+	+	+	+	−	+	+	+	+
Prominent eyes, proptosis	ND	ND	+	−	−	+	+	−	+	+	+	+
Blue sclerae	ND	ND	+	+	+	−	+	−	+	+	+	−
Long upper lip	ND	ND	−	+	+	−	+	+	+	+	+	−
Micrognathia	ND	ND	+	+	+	+	−	+	−	−	−	−
Cleft palate	ND	ND	−	−	−	−	−	−	−	−	−	+
Musculoskeletal												
Kyphoscoliosis[b]	+ (7 months)	+ (1.2 years)	+ (8 months)	+ (infancy)	+ (2 years)	+ (3 months)	+ (8 months)	+ (1 year)	+ (6 months)	++ (prenatal)	++ (prenatal)	++ (2 years)
Spatulate finger	−	ND	+	+	+	+	−	−	+	+	+	−
Finger laxity	ND	ND	+	+	−	−	+	−	++	+	+	+
Large joint laxity	ND	ND	+	+	−	−	+	−	++	++	++	+
Restricted elbow movement	+	ND	+	+	+	−	−	+	+	+	+	+
Hand contracture	−	−	−	−	−	+	−	−	−	+	+	−

(*Continued on next page*)

Table 1. *Continued*

Subject ID	P1	P2	P3	P4	P5	P6	P7	P8	P9	P10	P11	P12
Hip dislocation	–	–	–	+	–	+	–	–	–	+	+	+
Clubfeet	–	–	+	–	–	–	+	–	–	+	+	–
Muscular hypotonia	–	–	+	–	–	–	–	–	++	++	++	++
Skin and Hair												
Doughy skin	ND	ND	+	–	–	–	+	–	++	+	+	+
Hyperextensibility	ND	ND	+	–	–	–	+	–	++	+	+	–
Cutis laxa	ND	ND	–	–	–	–	–	–	+	+	–	+
Sparse hair	ND	ND	–	–	–	–	–	–	+	+	+	–
Others			MR, DD				camptodactyly			DD		pectus excavatum
Radiological Features												
Platyspondyly	+[c]	+[c]	+[c]	+	+	+	+	+	+	+	+	+
Anterior beak of vertebral body[b]	+	+	– (4 years)	– (5 years)	+	+	+	–	+	+	+	+
Short ilia	+	+	+	+	+	+	+	+	+	+	+	+
Prominent lesser trochanter	+	+	+	–	+	+	+	+	+	+	+	+
Metaphyseal flaring	+	+	+	+	+	+	+	+	+	–	+	+
Epiphyseal dysplasia of femoral head	–	–	–	+	–	+	–	–	–	–	+	+
Elbow malalignment	ND	ND	+	+	+	+	+	+	+	+	+	+
Advanced carpal ossification[b]	– (9 years)	ND	– (12 years)	+	+	+	+	ND	+	– (7 years)	–	– (5 years)
Carpal fusion	ND	ND	+	–	–	–	–	–	–	–	–	–
Metacarpal shortening	ND	ND	+	+	+	+	+	+	–	–	+	–
Overtubulation	–	–	–	–	–	–	–	–	+	+	+	+

Abbreviations are as follows: SEMD-JL1, spondyloepimetaphyseal dysplasia with joint laxity type 1; EDS-PF, Ehlers-Danlos syndrome, progeroid form; ND, no data; MR, mitral regurgitation; DD, developmental delay.
[a]At last presentation.
[b]Age at medical attention provided in parentheses.
[c]Absent at age 20 years in P1 and P2 and at age 12 years in P3.

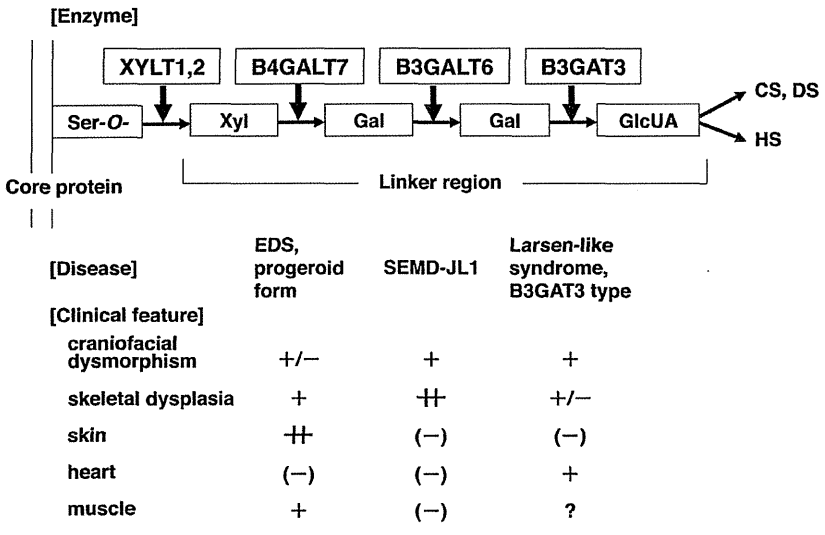

Figure 1. Enzymes Involved in Biosynthesis of the Glycosaminoglycan Linker Region and Summary Features of Diseases Caused by Their Defects Based on a Conventional Concept for the Diseases

The biosyntheses of GAGs start with the formation of a common tetrasaccharide linker sequence covalently attached to the core protein. The linker region synthesis involves a single linear pathway composed of four successive steps catalyzed by distinctive enzymes. Abbreviations are as follows: XYLT, β-xylosyltransferase; B4GALT7, xylosylprotein β1,4-galactosyltransferase, polypeptide 7 (β1,4-galactosyltransferase-I); B3GALT6, UDP-Gal, βGal β1,3-galactosyltransferase polypeptide 6 (β1,3-galactosyltransferase-II); B3GAT3, β-1,3-glucuronyltransferase 3 (glucuronosyltransferase I); Ser-*O*, the serine residue of the GAG attachment site on the proteoglycan core protein; Xyl, xylose; Gal, galactose; GlcUA, D-glucuronic acid; CS, chondroitin sulfate; DS, dermatan sulfate; HS, heparan sulfate; EDS, Ehlers-Danlos syndrome; SEMD-JL1, spondyloepimetaphyseal dysplasia with joint laxity type 1.

from peripheral blood, saliva, or Epstein-Barr virus-immortalized lymphocyte of the individuals with SEMD-JL1 and/or their parents after informed consent. The study was approved by the ethical committee of RIKEN and participating institutions. We captured the exomes of the seven subjects as previously described.[6,7] In brief, we sheared genomic DNA (3 μg) by Covaris S2 system (Covaris) and processed with a SureSelect All Exon V4 kit (Agilent Technologies). We sequenced DNAs captured by the kit with HiSeq 2000 (Illumina) with 101 base pair-end reads. We performed the image analysis and base calling by HiSeq Control Software/Real Time Analysis and CASAVA1.8.2 (Illumina) and mapped the sequences to human genome hg19 by Novoalign. We processed the aligned reads by Picard to remove PCR duplicate. The mean depth of coverage for reads was 132.8×, and, on average, 91.0% of targeted bases had sufficient coverage (20× coverage) and quality for variant calling (Table S1 available online). The variants were called by Genome Analysis Toolkit 1.5-21 (GATK) with the best practice variant detection with the GAKT v.3 and annotated by ANNOVAR (2012 February 23).

Based on the hypothesis that SEMD-JL1 is inherited in an autosomal-recessive fashion, we filtered variants with the script created by BITS (Tokyo, Japan) according to following conditions: (1) variants registered in ESP5400, (2) variants found in our in-house controls (n = 274), (3) synonymous changes, (4) rare variants registered in dbSNP build 135 (MAF < 0.01), and (5) variants associated with segmental duplication. After combining variants selected by the homozygous mutation model and the compound heterozygous mutation model, we selected genes shared by individuals from three or more families. The analysis of the next-generation sequencing identified possible compound heterozygous variants in *B3GALT6* in individuals from three families (Table S2). In addition, two other subjects had possible causal heterozygous variants of *B3GALT6*.

B3GALT6 (RefSeq accession number NM_080605.3) is a single-exon gene on chromosome 1p36.33. It encodes UDP-Gal:βGal β1,3-galactosyltransferase polypeptide 6 (or galactosyltransferase-II: GalT-II), an enzyme involved in the biosynthesis of the glycosaminoglycan (GAG) linker region.[8] The biosyntheses of dermatan sulfate (DS), chondroitin sulfate (CS), and heparin/heparan sulfate (HS) GAGs start with the formation of a tetrasaccharide linker sequence, glucuronic acid-β1-3-galactose-β1-3-galactose-β1-4-xylose-β1 (GlcUA-Gal-Gal-Xyl), which is covalently attached to the core protein. The linker region synthesis involves a single linear pathway composed of four successive steps catalyzed by distinctive enzymes (Figure 1). The first step is the addition of xylose to the hydroxy group of specific serine residues on the core protein by xylosyltransferases from UDP-Xyl, followed by two distinct galactosyltransferases (GalT-I and II) and a glucuronosyltransferase from UDP-Gal and UDP-GlcUA, respectively. The next hexosamine addition is critical because it determines which GAG (i.e., CS, DS, or HS) is assembled on the linker region. GalT-II encoded by *B3GALT6* functions in the third step of the linker formation (Figure 1).

To confirm the results obtained by the next-generation sequencing, we examined the seven subjects used for the next-generation sequencing and an additional subject from a Vietnamese family (F7) by direct sequence of the PCR products from genomic DNAs using 3730xl DNA Analyzer (Applied Biosystems). The Sanger sequencing confirmed all *B3GALT6* mutations found by the next-generation sequencing and identified additional *B3GALT6* mutations. The results indicated that *B3GALT6* mutations were found in all subjects (Tables 2 and S1). All but P4 from F3 were compound heterozygotes of missense mutations. In P4, only a heterozygous c.1A>G (p.Met1?) mutation was found, although we searched for a *B3GALT6* mutation in the entire coding region, 5′ and 3′ UTRs, and flanking

Table 2. *B3GALT6* Mutations in Spondyloepimetaphyseal Dysplasia with Joint Laxity Type 1 and Ehlers-Danlos Syndrome, Progeroid Form

Family	Clinical Diagnosis	Nucleotide Change	Amino Acid Change
F1	SEMD-JL1	c.1A>G	p.Met1?
		c.694C>T	p.Arg232Cys
F2	SEMD-JL1	c.1A>G	p.Met1?
		c.466G>A	p.Asp156Asn
F3[a]	SEMD-JL1	c.1A>G	p.Met1?
F4	SEMD-JL1	c.1A>G	p.Met1?
		c.694C>T	p.Arg232Cys
F5	SEMD-JL1	c.694C>T	p.Arg232Cys
		c.899G>C	p.Cys300Ser
F6	SEMD-JL1	c.1A>G	p.Met1?
		c.193A>G	p.Ser65Gly
F7	SEMD-JL1	c.200C>T	p.Pro67Leu
		c.694C>T	p.Arg232Cys
F8	EDS-PF	c.353delA	p.Asp118Alafs*160
		c.925T>A	p.Ser309Thr
F9	EDS-PF	c.588delG	p.Arg197Alafs*81
		c.925T>A	p.Ser309Thr
F10	EDS-PF	c.16C>T	p.Arg6Trp
		c.415_423del	p.Met139Ala141del

The nucleotide changes are shown with respect to *B3GALT6* mRNA sequence. The corresponding predicted amino acid changes are numbered from the initiating methionine residue.
[a]Only a heterozygous mutation was found.

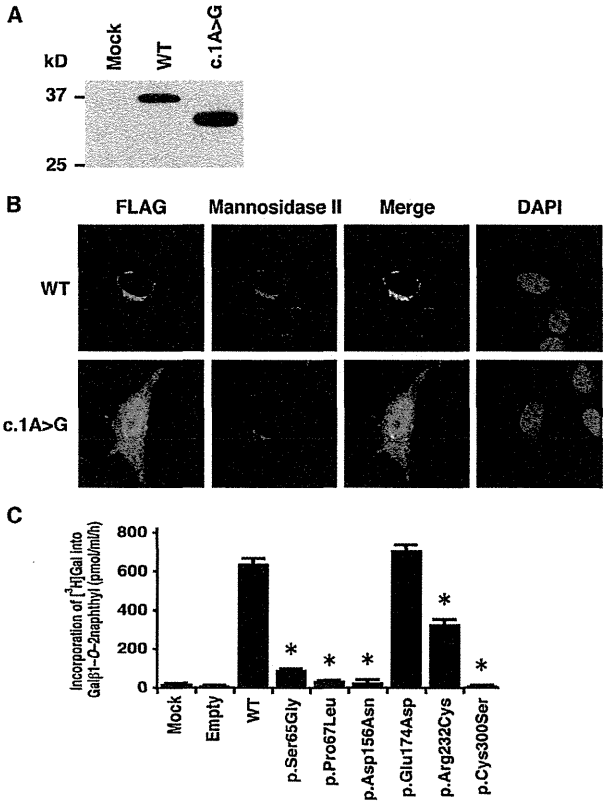

Figure 2. Analyses of B3GALT6 Missense Mutant Proteins Identified in Individuals with SEMD-JL1 In Vitro
(A) Immunoblot analysis of lysates from HeLa cells expressing transfected wild-type (WT) and mutant (c.1A>G) *B3GALT6*. The mutant *B3GALT6* yields a shortened protein. The difference of the molecular sizes between WT and mutant proteins is approximately ~4 kD.
(B) Subcellular localization of B3GALT6. HeLa cells were transfected with WT and mutant (c.1A>G) *B3GALT6*. Cells were stained with anti-FLAG (green), anti-α-mannosidase II (red), and 4′,6-diamidino-2-phenylindole (DAPI; blue). WT was expressed in the Golgi, but the mutant was found in cytoplasm and nucleus.
(C) Decreased enzyme activities of the missense mutant proteins (p.Ser65Gly, p.Pro67Lys, p.Asp156Asn, p.Arg232Cys, and p.Cys300Ser). p.Glu174Asp is a common polymorphism in the public database. The GalT-II activity is measured by incorporation of [^{3}H]Gal into Galβ1-*O*-2naphthyl (*p*mol/ml/hr) and represents the averages of three independent experiments performed in triplicate. Empty and mock indicate the GalT-II activity obtained with the conditioned medium transfected with or without an empty vector. *$p < 0.0001$ versus WT (one-way analysis of variance with Dunnett's adjustment).

regions of *B3GALT6*. Most of the mutations are predicted to be disease causing by in silico analysis. The c.1A>G (p.Met1?) mutation was found in individuals from five of the seven families.

Although mutations affecting initiation codons have been reported to be pathogenic in several diseases,[9] the effects of initiation codon mutations on the encoded protein are variable among the genes. We therefore investigated the effect of the c.1A>G (p.Met1?) mutation on the protein by using C-terminally FLAG-tagged B3GALT6 with and without the mutation expressed in HeLa cells (RIKEN Cell Bank). We detected the mutant B3GALT6 protein with a molecular weight ~4 kD lower compared with the wild-type (WT) protein (Figure 2A). These results suggest that translation initiation at the second ATG of the coding sequence, at position c.124, would become the initiation codon because of the mutation, probably resulting in an N-terminal deletion of 41 amino acids (p.Met1_Ala41del), in the same open reading frame that contains the transmembrane domain. We then examined the subcellular localization of the mutant B3GALT6 protein by immunocytochemistry. The immunofluorescence for WT-B3GALT6 was observed in a perinuclear region overlapping with that for α-mannosidase II, a marker of the Golgi as previously reported.[8] In contrast, the immunofluorescence for the mutant B3GALT6 protein was observed in the nucleus and cytoplasm (Figure 2B). Therefore, the mutant protein can be considered to be functionally null because of the mislocalization.

To investigate the causality of other *B3GALT6* missense mutations, we also examined the subcellular localization of the mutant B3GALT6 proteins by immunocytochemistry. c.193A>G (p.Ser65Gly), c.200C>T (p.Pro67Leu),

and c.694C>T (p.Arg232Cys) mutants showed mislocalization, whereas c.466G>A (p.Asp156Asn) and c.899G>C (p.Cys300Ser) mutants showed normal localization (Figure S1). To investigate whether the *B3GALT6* missense mutations affect the enzyme function, the GalT-II activities of soluble FLAG-tagged proteins for WT and mutant B3GALT6 proteins were assayed. The GalT-II activities of p.Ser65Gly-, p.Pro67Leu-, p.Asp156Asn-, p.Arg232Cys-, and p.Cys300Ser-B3GALT6 were significantly decreased compared with WT-B3GALT6 (Figure 2C), indicating that these mutations resulted in a loss of enzyme function. On the other hand, there were no significant differences in the GalT-II activities between WT-B3GALT6 and p.Glu174Asp-B3GALT6, a common polymorphism (rs12085009) in the public database (Figure 2C).

All SEMD-JL1 individuals with the *B3GALT6* mutation had the characteristic skeletal abnormalities, including platyspondyly, short ilia, and elbow malalignment (Table 1 and Figure S2); however, some had a range of extraskeletal and connective tissue abnormalities that overlapped with those seen in Ehlers-Danlos syndrome, progeroid form (EDS-PF [MIM 130070]). EDS-PF is an autosomal-recessive connective tissue disorder characterized by sparse hair, wrinkled skin, and defective wound healing with atrophic scars.[10] In addition, skeletal abnormalities so far reported in EDS-PF are limited to generalized osteopenia and radial head dislocation, which are in contrast with the severe generalized dysplasias of the axial and appendicular skeleton observed in SEMD-JL1. Thus, both disorders at first glance appear as separate clinical entities, although they share the clinical features of short stature, joint laxity and dislocation, and facial dysmorphism. In two families with individuals with EDS-PF, recessive mutations of *B4GALT7* (MIM 604327) have been found.[11,12] *B4GALT7* (RefSeq NM_007255.2) encodes an enzyme, xylosylated protein β-1,4-galactosyltransferase, that catalyzes the second step of the GAG linker region biosynthesis (Figure 1). Therefore, we speculated that B3GALT6 and B4GALT7 deficiencies might show similar phenotypes. We then examined *B3GALT6* in four additional individuals (P9–P12) who had phenotypes compatible with EDS-PF (Table 1 and Figure S3) but in whom no *B4GALT7* mutations had been found. Sanger sequencing of the EDS-PF-like subjects revealed that all were compound heterozygotes for *B3GALT6* mutations (Table 2). There were two frameshift mutations and one missense mutation (c.925T>A [p.Ser309Thr]) common in two families (F8 and F9). We investigated the enzyme function of the missense mutation by using the same assay for SEMD-JL1 missense mutations. The GalT-II activities of p.Ser309Thr-B3GALT6 were significantly decreased (Figure S4).

Collectively, 11 different mutations in individuals from 10 families were identified in *B3GALT6* by a combination of exome and targeted sequencing (Table 2 and Figure S5). None of these mutations were detected in more than 200 ethnicity-matched controls or in public databases, including the 1000 Genomes database, indicating that they are unlikely to be polymorphisms. SEMD-JL1 and EDS-PF-like individuals had no common mutations (Table 2). The individuals with *B3GALT6* mutations were short at birth and their short stature worsened with age. Their common clinical features were a flat face with prominent forehead and kyphoscoliosis (Table 1). Kyphoscoliosis was noticed in infancy in most cases and even in utero in severe cases. Although skeletal changes were essentially the same, craniofacial and skin abnormalities, joint laxities, and muscular hypotonia were variable among the individuals with *B3GALT6* mutations. Common radiographic features were platyspondyly that becomes less conspicuous with age, short ilia, and elbow malalignment (Table 1). Prominent lesser trochanters and metaphyseal flaring were seen in most cases. No individuals showed generalized osteoporosis. The disease phenotype was very variable between families (mutations), but in two familial cases, phenotypes were similar between the pair of the sibs. As a corollary, our results indicate that EDS-PF is genetically heterogeneous, with a proportion of cases being caused by mutations in *B4GALT7* and another in *B3GALT6*.

Diseases caused by defects in enzymes involved in the biosynthesis of the GAG linker region are categorized as the GAG linkeropathy. The first member of GAG linkeropathy has been identified to arise from an EDS-PF/B4GALT7 deficiency. *B4GALT7* mutations have been identified in homozygous c.808C>T (p.Arg270Cys)[12] and compound heterozygous (c.557C>A [p.Ala186Asp] and c.617T>C [p.Leu206Pro])[11] states. Another member of GAG linkeropathy manifests itself as Larsen-like syndrome, B3GAT3 type (MIM 245600). A family with individuals harboring a homozygous *B3GAT3* (MIM 606374; RefSeq NM_012200.3) mutation (c.830G>A [p.Arg227Gln]) has been identified. The clinical features of five affected individuals of the family are characterized by dislocation and laxity of joints and congenital heart defects.[11] The former considerably overlaps with the phenotypes of SEMD-JL1 and EDS-PF, two other GAG linkeropathies; however, the association of heart defects has critically differentiated this disease from the others (Figure 1).

Given that the linker region biosynthesis is nonparallel and that the defects in the three enzymes simply affect the amounts of the linker region available to form GAGs (CS, HS, DS), phenotypic similarities of the three diseases are quite understandable. The quantitative difference of the phenotypes (severity of the diseases) most probably results from the difference in the degree of enzyme defects resulting from mutations. On the other hand, qualitative differences of the three diseases (e.g., scoliosis caused by the *B3GALT6* mutation, heart disease caused by the *B3GAT3* mutation, etc.) suggest other explanations. Tissue expression patterns of the three genes do not entirely explain the differences. We examined their mRNA expression in various human tissues, including cartilage, bone, and connective tissues by quantitative real-time PCR (Figure S6). We detected strong expression of *B3GALT6* in

Table 3. The Amount of GAGs in the Lymphoblastoid Cells from Individuals with Spondyloepimetaphyseal Dysplasia with Joint Laxity Type 1

	GAG (Disaccharides/mg Acetone Powder)[a] [pmol]			
Subject	**CS/DS**	**CS**	**DS**	**HS**
Control	62	48	29	128
SEMD-JL1				
P1	313	295	118	15
P2	345	175	60	21
P3	270	162	28	20

[a]Calculated based on the peak area in chromatograms of digests with a mixture of chondroitinases ABC and AC-II (CS/DS), chondroitinases AC-I and AC-II (CS), chondroitinase B (DS), and heparinases I and III (HS).

cartilage and bone but only weak expression in skin, ligament, and tendon. *B4GALT7* expression was stronger in cartilage than *B3GALT6* and also weak in skin and ligament. *B3GAT3* expression was not specific to heart. The qualitative difference may result from the difference in the effects of the three genes on GAG formation.

To examine how *B3GALT6* mutations affects the products of GAGs in vivo, we measured the amounts of CS and HS chains at the surface of lymphoblastoid cells from the subjects by flow cytometry by using CS-stub and HS-stub antibodies as previously described.[13–15] In brief, purified GAG fractions were treated individually with a mixture of chondroitinases ABC and AC-II, a mixture of chondroitinases AC-I (EC 4.2.2.5) (Seikagaku Corp.) and AC-II (EC 4.2.2.5) (Seikagaku Corp.), chondroitinase B (EC 4.2.2.19) (IBEX Technologies), or a mixture of heparinases-I and -III (IBEX Technologies) for analyzing the disaccharide composition of CS/DS, CS, DS, and HS, respectively. The digests were labeled with a fluorophore 2-aminobenzamide (2AB) and aliquots of the 2AB derivatives of CS/DS/HS disaccharides were analyzed by anion-exchange HPLC on a PA-03 column (YMC Co.). The HS-stub antibody (3G10) showed a markedly reduced binding to the epitopes on the subjects' cells (Figure S7). The relative numbers of the HS chains presented as the mean fluorescence intensity (MFI) of the cell population stained with the antibody for P1, P2, and P3 were 26%, 56%, and 35% of the control, respectively. On the other hand, the CS-stub antibody (2B6) showed a similar binding to the epitopes on the subjects' cells relative to those of the control (Figure S7). The MFI for P1, P2, and P3 were 114%, 104%, and 106% of the control, respectively. Furthermore, we measured disaccharide of GAG chains from lymphoblastoid cells by using anion-exchange HPLC after digestion with chondroitinase and heparinase. The amounts of the disaccharide from HS chains were significantly decreased, whereas CS and DS chains were ~5 times higher than those in the control (Table 3).

Previous biochemical studies on EDS-PF with *B4GALT7* mutations show a reduction in the synthesis of DS chains.[16,17] The c.830G>A (p.Arg227Gln) mutation in *B3GAT3* causes a drastic reduction in GlcAT-I activity in fibroblasts of the individual with SEMD-JL1 and numbers of CS and HS chains on the core proteins at the surface of the fibroblasts are decreased to about half of the controls.[11] Cultured lymphoblastoid cells from individuals with a c.419C>T (p.Pro140Leu) mutation in *B3GAT3* show that defective synthesis is more pronounced for CS than for HS.[11] Taken together with our results, these findings suggest that the effects of the deficiencies of the three enzymes on GAG synthesis are not identical. A possible explanation for the qualitative phenotypic differences may be that the biosynthesis of the GAG linker region is not a simple step-by-step addition but involves parallel processing and/or alternative pathways. Other glycosyltransferases may have similar biochemical functions to these three enzymes and thus complement their deficient activities to variable degrees in cell- and/or tissue-specific manners, leading to differences in the amount of GAGs in the tissues. It is known that B3GALT6 and B4GALT7 have several homologs.[18] It must be noted that all biochemical studies so far have been performed in vitro or in cultured cells, and therefore there is a severe limitation to our understanding of the pathogenesis at tissue and organ levels.

By exome sequencing, we identified loss-of-function mutations in *B3GALT6* in 12 individuals from 10 families. The mutations produced a spectrum of connective tissue disorders characterized by lax skin, muscle hypotonia, joint dislocation, and skeletal dysplasia and deformity, which include phenotypes previously known as SEMD-JL1 and EDS-PF (Figures S1 and S2). The pleiotropic phenotypes of *B3GALT6* mutations indicate that B3GALT6 plays critical roles in development and homeostasis of various tissues, including skin, bone, cartilage, tendons, and ligaments. Biochemical studies that used lymphoblastoid cells of the individuals with *B3GALT6* mutations showed a decrease of HS and a paradoxical increase of CS and DS of the cell surface. Further clinical, genetic, and biological studies are necessary to understand the pathological mechanism of the diseases caused by enzyme defects involved in the biosynthesis of the GAG linker region and roles of the region in GAG metabolism and function.

Supplemental Data

Supplemental Data include seven figures and two tables and can be found with this article online at http://www.cell.com/AJHG/.

Acknowledgments

We thank the individuals with the disease and their family for their help to the study. We also thank the Japanese Skeletal Dysplasia Consortium. This study is supported by research grants from the Ministry of Health, Labor, and Welfare (23300101 to S.I. and N. Matsumoto; 23300201 to S.I.), by Grants-in-Aid for Young Scientists (23689052 to N. Miyake and 23790066 to S.M.) from the Japan Society for the Promotion of Science; by the Matching Program for Innovations in Future Drug Discovery and Medical Care

(K.S.); by The Ministry of Education, Culture, Sports, Science and Technology, Japan (MEXT); by a Grant-in-aid for Encouragement from the Akiyama Life Science Foundation (S.M.); by Swiss National Science Foundation Grants (31003A_141241 and 310030_132940); by The CoSMO-B project (Brazil and Switzerland); by the Leenaards Foundation (Switzerland); and by Research on intractable diseases, Health and Labour Sciences Research Grants, H23-Nanchi-Ippan-123 (S.I.).

Received: February 1, 2013
Revised: March 16, 2013
Accepted: April 5, 2013
Published: May 9, 2013

Web Resources

The URLs for data presented herein are as follows:

1000 Genomes, http://browser.1000genomes.org
ANNOVAR, http://www.openbioinformatics.org/annovar/
dbSNP, http://www.ncbi.nlm.nih.gov/projects/SNP/
GATK, http://www.broadinstitute.org/gatk/
MutationTaster, http://www.mutationtaster.org/
NHLBI Exome Sequencing Project (ESP) Exome Variant Server, http://evs.gs.washington.edu/EVS/
Novoalign, http://www.novocraft.com/main/page.php?s=novoalign
Online Mendelian Inheritance in Man (OMIM), http://www.omim.org/
Picard, http://picard.sourceforge.net/
PolyPhen, http://www.genetics.bwh.harvard.edu/pph2/
RefSeq, http://www.ncbi.nlm.nih.gov/RefSeq
SIFT, http://sift.bii.a-star.edu.sg/
UCSC Genome Browser, http://genome.ucsc.edu

References

1. Warman, M.L., Cormier-Daire, V., Hall, C., Krakow, D., Lachman, R., LeMerrer, M., Mortier, G., Mundlos, S., Nishimura, G., Rimoin, D.L., et al. (2011). Nosology and classification of genetic skeletal disorders: 2010 revision. Am. J. Med. Genet. A. *155A*, 943–968.
2. Beighton, P., Gericke, G., Kozlowski, K., and Grobler, L. (1984). The manifestations and natural history of spondylo-epimetaphyseal dysplasia with joint laxity. Clin. Genet. *26*, 308–317.
3. Nishimura, G., Satoh, M., Aihara, T., Aida, N., Yamamoto, T., and Ozono, K. (1998). A distinct subtype of "metatropic dysplasia variant" characterised by advanced carpal skeletal age and subluxation of the radial heads. Pediatr. Radiol. *28*, 120–125.
4. Boyden, E.D., Campos-Xavier, A.B., Kalamajski, S., Cameron, T.L., Suarez, P., Tanackovic, G., Andria, G., Ballhausen, D., Briggs, M.D., Hartley, C., et al. (2011). Recurrent dominant mutations affecting two adjacent residues in the motor domain of the monomeric kinesin KIF22 result in skeletal dysplasia and joint laxity. Am. J. Hum. Genet. *89*, 767–772.
5. Min, B.J., Kim, N., Chung, T., Kim, O.H., Nishimura, G., Chung, C.Y., Song, H.R., Kim, H.W., Lee, H.R., Kim, J., et al. (2011). Whole-exome sequencing identifies mutations of KIF22 in spondyloepimetaphyseal dysplasia with joint laxity, leptodactylic type. Am. J. Hum. Genet. *89*, 760–766.
6. Miyake, N., Elcioglu, N.H., Iida, A., Isguven, P., Dai, J., Murakami, N., Takamura, K., Cho, T.J., Kim, O.H., Hasegawa, T., et al. (2012). PAPSS2 mutations cause autosomal recessive brachyolmia. J. Med. Genet. *49*, 533–538.
7. Tsurusaki, Y., Okamoto, N., Ohashi, H., Kosho, T., Imai, Y., Hibi-Ko, Y., Kaname, T., Naritomi, K., Kawame, H., Wakui, K., et al. (2012). Mutations affecting components of the SWI/SNF complex cause Coffin-Siris syndrome. Nat. Genet. *44*, 376–378.
8. Bai, X., Zhou, D., Brown, J.R., Crawford, B.E., Hennet, T., and Esko, J.D. (2001). Biosynthesis of the linkage region of glycosaminoglycans: cloning and activity of galactosyltransferase II, the sixth member of the beta 1,3-galactosyltransferase family (beta 3GalT6). J. Biol. Chem. *276*, 48189–48195.
9. Saunders, C.J., Minassian, B.E., Chow, E.W., Zhao, W., and Vincent, J.B. (2009). Novel exon 1 mutations in MECP2 implicate isoform MeCP2_e1 in classical Rett syndrome. Am. J. Med. Genet. A. *149A*, 1019–1023.
10. Kresse, H., Rosthøj, S., Quentin, E., Hollmann, J., Glössl, J., Okada, S., and Tønnesen, T. (1987). Glycosaminoglycan-free small proteoglycan core protein is secreted by fibroblasts from a patient with a syndrome resembling progeroid. Am. J. Hum. Genet. *41*, 436–453.
11. Baasanjav, S., Al-Gazali, L., Hashiguchi, T., Mizumoto, S., Fischer, B., Horn, D., Seelow, D., Ali, B.R., Aziz, S.A., Langer, R., et al. (2011). Faulty initiation of proteoglycan synthesis causes cardiac and joint defects. Am. J. Hum. Genet. *89*, 15–27.
12. Faiyaz-Ul-Haque, M., Zaidi, S.H., Al-Ali, M., Al-Mureikhi, M.S., Kennedy, S., Al-Thani, G., Tsui, L.C., and Teebi, A.S. (2004). A novel missense mutation in the galactosyltransferase-I (B4GALT7) gene in a family exhibiting facioskeletal anomalies and Ehlers-Danlos syndrome resembling the progeroid type. Am. J. Med. Genet. A. *128A*, 39–45.
13. Kinoshita, A., and Sugahara, K. (1999). Microanalysis of glycosaminoglycan-derived oligosaccharides labeled with a fluorophore 2-aminobenzamide by high-performance liquid chromatography: application to disaccharide composition analysis and exosequencing of oligosaccharides. Anal. Biochem. *269*, 367–378.
14. Miyake, N., Kosho, T., Mizumoto, S., Furuichi, T., Hatamochi, A., Nagashima, Y., Arai, E., Takahashi, K., Kawamura, R., Wakui, K., et al. (2010). Loss-of-function mutations of CHST14 in a new type of Ehlers-Danlos syndrome. Hum. Mutat. *31*, 966–974.
15. Mizumoto, S., and Sugahara, K. (2012). Glycosaminoglycan chain analysis and characterization (Glycosylation/Epimerization). In Methods in Molecular Biology. In Proteoglycans: Methods and Protocols, F. Rédini, ed. (New York, USA: Humana Press, Springer), pp. 99–115.
16. Okajima, T., Fukumoto, S., Furukawa, K., and Urano, T. (1999). Molecular basis for the progeroid variant of Ehlers-Danlos syndrome. Identification and characterization of two mutations in galactosyltransferase I gene. J. Biol. Chem. *274*, 28841–28844.
17. Quentin, E., Gladen, A., Rodén, L., and Kresse, H. (1990). A genetic defect in the biosynthesis of dermatan sulfate proteoglycan: galactosyltransferase I deficiency in fibroblasts from a patient with a progeroid syndrome. Proc. Natl. Acad. Sci. USA *87*, 1342–1346.
18. Togayachi, A., Sato, T., and Narimatsu, H. (2006). Comprehensive enzymatic characterization of glycosyltransferases with a beta3GT or beta4GT motif. Methods Enzymol. *416*, 91–102.

Epilepsia, 54(7):1262–1269, 2013
doi: 10.1111/epi.12203

FULL-LENGTH ORIGINAL RESEARCH

Targeted capture and sequencing for detection of mutations causing early onset epileptic encephalopathy

*Hirofumi Kodera, †Mitsuhiro Kato, ‡[1]Alex S. Nord, ‡Tom Walsh, ‡Ming Lee, §Gaku Yamanaka, ¶Jun Tohyama, *†Kazuyuki Nakamura, #Eiji Nakagawa, **Tae Ikeda, ††Bruria Ben-Zeev, ‡‡Dorit Lev, ‡‡Tally Lerman-Sagie, §§Rachel Straussberg, ¶¶Saori Tanabe, ##Kazutoshi Ueda, ***Masano Amamoto, †††Sayaka Ohta, ‡‡‡Yutaka Nonoda, *Kiyomi Nishiyama, *Yoshinori Tsurusaki, *Mitsuko Nakashima, *Noriko Miyake, †Kiyoshi Hayasaka, ‡Mary-Claire King, *Naomichi Matsumoto, and *Hirotomo Saitsu

*Department of Human Genetics, Yokohama City University Graduate School of Medicine, Yokohama, Japan; †Department of Pediatrics, Yamagata University Faculty of Medicine, Yamagata, Japan; ‡Department of Genome Sciences and Department of Medicine, University of Washington, Seattle, Washington, U.S.A.; §Department of Pediatrics, Tokyo Medical University, Tokyo, Japan; ¶Department of Pediatrics, Nishi-Niigata Chuo National Hospital, Niigata, Japan; #Department of Child Neurology, National Center of Neurology and Psychiatry, Tokyo, Japan; **Division of Pediatric Neurology, Osaka Medical Center and Research Institute for Maternal and Child Health, Osaka, Japan; ††The Edmond and Lily Safra Children's Hospital, Sheba Medical Center, Ramat Gan, Israel; ‡‡Metabolic Neurogenetic Clinic, Wolfson Medical Center, Holon, Israel; §§Department of Neurogenetics, Schneider's Children Medical Center, Petah Tiqwa, Israel; ¶¶Department of Pediatrics, Nihonkai General Hospital, Sakata, Japan; ##Department of Pediatrics, Kitano Hospital, Osaka, Japan; ***Pediatric Emergency Center, Kitakyusyu City Yahata Hospital, Kitakyushu, Japan; †††Department of Pediatrics, Graduate School of Medicine, University of Tokyo, Tokyo, Japan; and ‡‡‡Department of Pediatrics, School of Medicine, Kitasato University, Sagamihara, Japan

Summary

Purpose: Early onset epileptic encephalopathies (EOEEs) are heterogeneous epileptic disorders caused by various abnormalities in causative genes including point mutations and copy number variations (CNVs). In this study, we performed targeted capture and sequencing of a subset of genes to detect point mutations and CNVs simultaneously.

Methods: We designed complementary RNA oligonucleotide probes against the coding exons of 35 known and potential candidate genes. We tested 68 unrelated patients, including 15 patients with previously detected mutations as positive controls. In addition to mutation detection by the Genome Analysis Toolkit, CNVs were detected by the relative depth of coverage ratio. All detected events were confirmed by Sanger sequencing or genomic microarray analysis.

Key Findings: We detected all positive control mutations. In addition, in 53 patients with EOEEs, we detected 12 pathogenic mutations, including 9 point mutations (2 nonsense, 3 splice-site, and 4 missense mutations), 2 frameshift mutations, and one 3.7-Mb microdeletion. Ten of the 12 mutations occurred de novo; the other two had been previously reported as pathogenic. The entire process of targeted capture, sequencing, and analysis required 1 week for the testing of up to 24 patients.

Significance: Targeted capture and sequencing enables the identification of mutations of all classes causing EOEEs, highlighting its usefulness for rapid and comprehensive genetic testing.

KEY WORDS: Target capture, Sequencing, Mutation, Copy number variation, Genetic testing.

Early onset epileptic encephalopathies (EOEEs), occurring before 1 year of age, are characterized by impairment of cognitive, sensory, and motor development by recurrent clinical seizures or prominent interictal epileptiform discharges (Berg et al., 2010). Ohtahara syndrome (OS), West syndrome (WS), early myoclonic encephalopathy (EME), migrating partial seizures in infancy (MPSI), and Dravet syndrome (DS) are the best known epileptic encephalopathies recognized by the International League Against Epilepsy (ILAE; Berg et al., 2010). However, many infants with similar features do not strictly fit the parameters of these syndromes.

To date, 11 genes have been shown to be associated with EOEEs (Mastrangelo & Leuzzi, 2012). The identification of

Accepted March 21, 2013; Early View publication May 10, 2013.
Address correspondence to Hirotomo Saitsu, Department of Human Genetics, Yokohama City University Graduate School of Medicine, 3-9 Fukuura, Kanazawa-ku, Yokohama 236-0004, Japan. E-mail: hsaitsu@yokohama-cu.ac.jp
[1]Present address: Genomics Division, Lawrence Berkeley National Laboratory, Berkeley, California, U.S.A.

causative mutations associated with EOEEs and their related phenotypes is useful for genetic counseling, and possibly for management of the patients; however, it is time-consuming and arduous to screen all known disease-causing genes one by one using Sanger sequencing or high-resolution melting curve analysis (Wittwer, 2009). In addition, copy number variations (CNVs) involving causative genes can also cause EOEEs (Saitsu et al., 2008; Mei et al., 2010; Saitsu et al., 2011, 2012b). Array comparative genomic hybridization (CGH) and multiplex ligation-dependent probe amplification (MLPA) are well established for the detection of CNVs; however, it is often difficult for array CGH to detect small CNVs such as a single-exon deletion and for MLPA to screen multiple genes at a time (Schouten et al., 2002; Dibbens et al., 2011; Mefford et al., 2011; Stuppia et al., 2012). Therefore, an integrated method that detects both point mutations and CNVs for multiple genes would be useful for comprehensive genetic testing in EOEEs.

Recent progress in massively parallel DNA sequencing in combination with target capturing has facilitated rapid mutation detection (Ng et al., 2009). It has been reported that CNVs involving disease-causing genes in patients with breast or ovarian cancer can be detected by target capture sequencing using the relative depth of coverage ratio (Walsh et al., 2010, 2011; Nord et al., 2011). Targeted capture and sequencing of patients with epileptic disorders has successfully identified potential disease-causing mutations in 16 of 33 patients (Lemke et al., 2012), revealing its efficacy for detecting mutations. However, the detection of both point mutations and CNVs has not been reported in patients with epilepsy.

In this study, we performed targeted capture and sequencing of a subset of 35 genes to detect mutations and CNVs simultaneously in 68 patients with EOEEs. By analyzing the relative depth of coverage ratio, we were able to detect microdeletions, in which the numbers of deleted exons varied from a single exon to all exons of two genes. In combination with rapid sequencing using a benchtop next-generation sequencer, our method provides a fast, comprehensive, and cost-effective method for genetic testing of patients with EOEE.

Methods

Patients

We examined 68 patients (36 male and 32 female) with EOEEs (20 patients with OS, 20 with WS, 3 with EME, 4 with MPSI, 2 with DS, and 19 with unclassified epileptic encephalopathy). Diagnoses were based on clinical features and characteristic patterns on electroencephalography. In 15 of 68 patients (10 male and five female), disease-causing mutations or CNVs had been previously identified in our laboratory, so these mutations were used as positive controls (Table 1) (Saitsu et al., 2008, 2010a,b, 2011, 2012b,c; Nonoda et al., 2013). Genomic DNA was isolated from blood leukocytes according to standard methods. Experimental protocols were approved by the Yokohama City University School of Medicine Institutional Review Board for Ethical Issues. Written informed consent for genetic testing was obtained from the guardians of all tested individuals prior to analysis.

Target capture sequencing and variant detection

A custom-made SureSelect oligonucleotide probe library (Agilent Technologies, Santa Clara, CA, U.S.A.) was designed to capture the coding exons of 35 genes; 5 of them were potential candidates for EOEEs based on unpublished data (for a list of the 30 of 35 genes, see Table 2). We designed 120-bp capture probes with 3× centered probe-tiling, and avoiding 20-bp overlap to repeat region using the Agilent e-Array Web-based design tool. To cover regions

Table 1. Known mutations and copy number variants used as positive controls

	Case	Sex	Chr	Genes	Reported mutations or copy number variants (positive controls)	Type	Deletion size (kb)	Refs
SNVs	27	F	9	*STXBP1*	c.1328T>G (p.Met443Arg)	Missense		Saitsu et al. (2008)
	69	M	X	*CASK*	c.1A>G	Missense		Saitsu et al. (2012b)
	241	M	X	*CDKL5*	c.145G>A (p.Glu49Lys)	Missense		–
Indels	95	M	9	*STXBP1*	c.388_389del (p.Leu130AspfsX11)	Deletion		Saitsu et al. (2010a)
	313	M	X	*CASK*	c.227_228del (p.Glu76ValfsX6)	Deletion		–
	26	F	9	*SPTAN1*	c.6619_6621del (p.Glu2207del)	Deletion		Saitsu et al. (2010b)
	220	M	9	*STXBP1*	c.1381_1390del (p.Lys461GlyfsX82)	Deletion		–
	16	M	9	*SPTAN1*	c.6923_6928dup (p.Arg2308_Met2309dup)	Duplication		Saitsu et al. (2010b)
	309	M	9	*SPTAN1*	c.6908_6916dup (p.Asp2303_Leu2305dup)	Duplication		Nonoda et al. (2013)
CNVs	12	F	9	*STXBP1, SPTAN1*	Del(9)(q33.33–q34.11)	Microdeletion	2150	Saitsu et al. (2008)
	22	M	9	*STXBP1*	*STXBP1* Ex4 deletion	Microdeletion	4.6	Saitsu et al. (2011)
	83	M	X	*CASK*	*CASK* Ex2 deletion	Microdeletion	111	Saitsu et al. (2012b)
	102	F	X	*MECP2*	Del(X)(q28)	Microdeletion		–
	204	M	9	*STXBP1, SPTAN1*	Del(9)(q33.33–q34.11)	Microdeletion	2850	Saitsu et al. (2011)
	214	F	X	*CDKL5*	Del(X)(q22.13)	Microdeletion	137	Saitsu et al. (2011)

SNVs, single nucleotide variants; Indels, insertion/deletions; CNVs, copy number variations.

Table 2. Sequence performance for 30 target genes

Gene	Cytoband	No. of coding exons	Mean read depth	%bases above 5× depth (%)	%bases above 10× depth (%)
ARHGEF9	Xq11.1–q11.2	10	206	100	100
ARX	Xp21.3	5	44	59.4–94.4	38.7–90.6
CASK	Xp11.4	27	201	95.9–100	95.9–100
CDKL5	Xp22.13	20	238	100	100
COL4A1	13q34	52	287	98.3–100	98.3–100
COL4A2	13q34	47	190	100	99.1–100
FOXG1	14q12	1	231	86.5–100	81.1–96.4
GABRG2	5q34	11	300	92.3	92.3
GRIN2A	16p13.2	13	310	100	100
KCNQ2	20q13.33	17	135	100	97.7–100
MAGI2	7q21.11	22	255	96–98.3	94.5–97.5
MAPK10	4q21.3	12	304	100	100
MECP2	Xq28	3	217	96.2	96.2
MEF2C	5q14.3	10	270	100	100
NTNG1	1p13.3	9	298	100	100
PCDH19	Xq22.1	6	212	100	100
PLCB1	20p12.3	32	293	100	100
PNKP	19q13.33	17	208	100	98.5–100
PNPO	17q21.32	7	210	100	100
SCN1A	2q24.3	26	345	100	100
SCN2A	2q24.3	26	323	100	100
SLC25A22	11p15.5	9	121	100	100
SLC2A1	1p34.2	10	209	100	98.8–100
SNPH	20p13	4	179	100	100
SPTAN1	9q34.11	56	277	100	100
SRGAP2	1q32.1	20	320	96.6	96.6
ST3GAL5	2p11.2	8	302	93.6–100	93.6–99.9
STXBP1	9q34.11	20	306	100	100
SYN1	Xp11.23	13	131	93.4–100	81–100
SYP	Xp11.23	6	146	100	99.1–100

where we could not design probes with the above settings, some probes from the SureSelect Human All Exon 50-Mb kit (Agilent Technologies) were added to the probe libraries. A total of 2,738 probes, covering 156 kb, were prepared. Exon capture, enrichment, and indexing were performed according to the manufacturer's instructions. Twenty-four captured libraries were mixed and sequenced on an Illumina MiSeq (Illumina, San Diego, CA, U.S.A.) with 150-bp paired-end reads. Image analysis and base calling were performed using the Illumina Real Time Analysis Pipeline version 1.13 and CASAVA software v.1.8 (Illumina) with default parameters. Sequence reads were aligned to the reference human genome (GRCh37: Genome Reference Consortium human build 37) with Novoalign (Novocraft Technologies, Selangor, Malaysia). After conversion of the SAM file to a BAM file with SAMtools (Li et al., 2009), duplicate reads were marked using Picard (http://picard.sourceforge.net/) and excluded from downstream analysis. Local realignment around insertion/deletions (indels) and base quality score recalibration were performed using the Genome Analysis Toolkit (DePristo et al., 2011). Single-nucleotide variants (SNVs) and indels were identified using the Genome Analysis Toolkit UnifiedGenotyper and filtered according to the Broad Institute's best-practice guidelines v.3 except for HaplotypeScore filtering. We excluded variants found in 147 exomes from healthy individuals previously sequenced in our laboratory. Variants were annotated using ANNOVAR (Wang et al., 2010). Candidate disease-causing mutations were confirmed by Sanger sequencing on a 3500xL Genetic Analyzer (Applied Biosystems, Foster City, CA, U.S.A.). The Human Gene Mutation Database professional 2012.3 (BIOBASE GmbH, Wolfenbuettel, Germany) was used to check whether the variants had been previously reported.

Copy number analysis using target capture sequence data

Copy number changes were analyzed based on the relative depth of coverage ratios (Nord et al., 2011). Raw coverage on the target regions was calculated by SAMtools using BAM files, in which duplicate reads were excluded. Raw coverage was normalized and corrected for GC content and bait capture bias. Next, the ratios were calculated by comparing the sample-corrected coverage to the median-corrected coverage for the other 23 samples. A sliding window (20 bp) was used to identify CNVs for which the majority of bases had a ratio ≤ 0.6 (loss) or ≥ 1.4 (gain). We visually inspected the ratio

data and judged whether the call was true or likely to be a false positive. A flow chart of our variant detection and copy number analysis scheme is illustrated in Fig. S1.

Genomic microarray analysis and cloning of deletion breakpoints

The microdeletion involving *SCN1A* and *SCN2A* was confirmed using a CytoScan HD Array (Affymetrix, Santa Clara, CA, U.S.A.) according to the manufacturer's protocol. Copy number alterations were analyzed using the Chromosome Analysis Suite (ChAS; Affymetrix) with NA32 (hg19) annotations. The junction fragment spanning the deletion was amplified by long polymerase chain reaction (PCR) using several primer sets based on putative breakpoints according to the microarray data. Long PCR was performed in a 20-μl volume, containing 30 ng genomic DNA, 1× buffer for KOD FX, 0.4 mM each dNTP, 0.3 μM each primer, and 0.3 U KOD FX polymerase (Toyobo, Osaka, Japan). The deletion junction fragments were obtained using the following primers: #409-F (5′-TCCACAGTTTACAAACATCTTTTCATGG-3′) and #409-R (5′-AGAAATTGGCTTGGTCAGTACCAGCA-3′) (1.6-kb amplicon). PCR products were electrophoresed on agarose gels stained with ethidium bromide, purified with ExoSAP (USB Technologies, Cleveland, OH, U.S.A.), and sequenced with BIGDYE TERMINATOR CHEMISTRY v.3 according to the manufacturer's protocol (Applied Biosystems).

Results

Target capture sequencing yielded an average of 26 Mb per sample (range 17–41 Mb per sample) on the target regions, resulting in an average read depth of 255 (range across all samples: 173–437). The coverage of the protein-coding sequences of the 30 target genes is shown in Table 2. Overall, 98.6% of targeted coding sequence bases were covered by 10 reads or more; however, some genes such as *ARX* and *FOXG1* were less well covered because of embedded repeat sequences (Fig. S2). To validate the performance of target capture sequencing for detecting mutations and CNVs, we analyzed 15 samples in which disease-causing mutations or microdeletions had been identified previously in our laboratory (Saitsu et al., 2008, 2010a,b, 2011, 2012b; Nonoda et al., 2013). All nine control point mutations and six control microdeletions were detected (Table 1; Fig. 1). These data indicate that our target capture sequencing method was able to detect both point mutations and microdeletions, including deletion of a single exon.

Examination of 53 previously unresolved EOEE patients by targeted capture and sequencing revealed mutations in 12 patients (Table 3). Every patient harbored a different

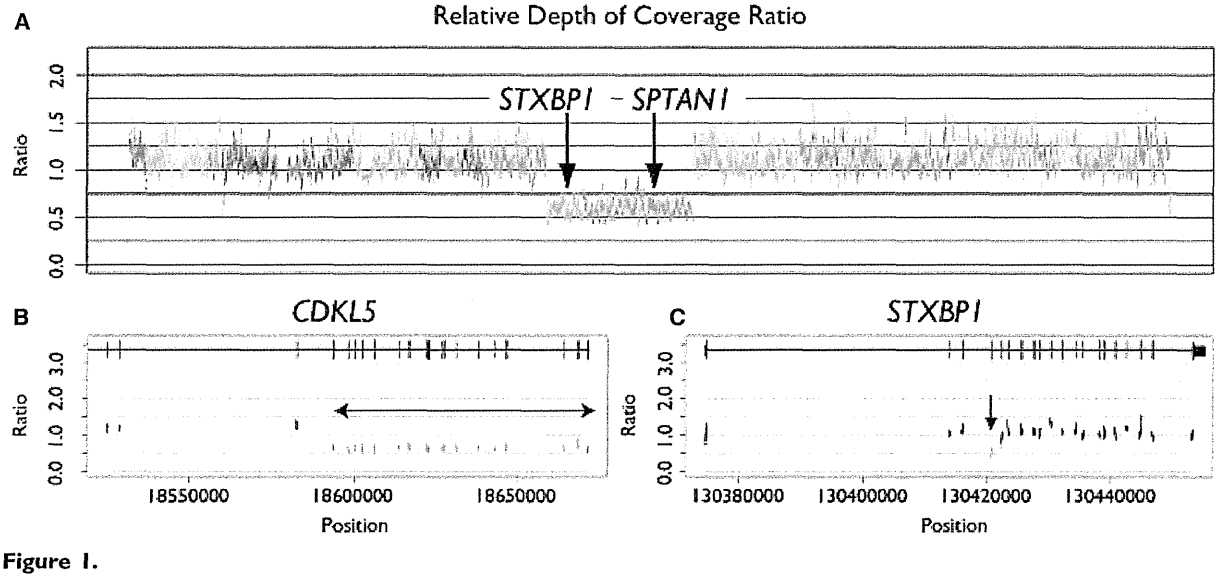

Figure 1.
Detection of three known microdeletions by target capture sequencing. (**A**) Relative depth of coverage ratio for patient 12. Coverage ratios for each target gene are indicated by different colors. A microdeletion including *STXBP1* and *SPTAN1* is clearly observed. (**B, C**) Relative depth of coverage ratio for patient 214 in the *CDKL5* region and patient 22 in the *STXBP1* region, respectively. Black vertical lines indicate exons and horizontal lines indicate introns (top). Red vertical lines show bait regions that were judged to be "deleted." A number of exons of *CDKL5* were deleted in patient 214 (bidirectional arrow in **B**), and a single exon of *STXBP1* was deleted in patient 22 (arrow in **C**).

Table 3. Mutations in 53 patients with EOEEs detected by targeted capture and sequencing

	Case	Sex	Diagnosis	Chr	Gene	Mutation	Type	Deletion size (kb)	Inheritance	References
SNVs	329	M	OS/EME	9	*STXBP1*	c.247-2A>G	Splice site		De novo	–
	402	M	OS	9	*STXBP1*	c.902+1G>A	Splice site		De novo	Milh et al. (2011)
	423	F	OS	9	*STXBP1*	c.246+1G>A	Splice site		De novo	–
	403	F	MAE or DS	2	*SCN1A*	c.580G>A (p.Asp194Asn)	Missense		Not found in the mother	Mancardi et al. (2006)
	415	F	EOEE	2	*SCN1A*	c.3714A>C (p.Glu1238Asp)	Missense		Not determined	Harkin et al. (2007)
	416	M	EOEE	X	*CDKL5*	c.533G>A (p.Arg178Gln)	Missense		De novo	Liang et al. (2011)
	418	F	WS, severe hypotonia	2	*SCN2A*	c.632G>A (p.Gly211Asp) in NM_001040143 (variant 3)	Missense		De novo	–
	244	F	Epilepsy + PCH	X	*CASK*	c.55G>T (p.Gly19X)	Nonsense		De novo	–
	404	F	EOEEs	X	*MECP2*	c.844C>T (p.Arg282X)	Nonsense		De novo	–
Indels	336	F	OS	9	*STXBP1*	c.1056del (p.Asp353ThrfsX3)	Deletion		De novo	–
	397	F	DS	2	*SCN1A*	c.342_344delinsAGGAGTT (p.Phe114LeufsX6)	Deletion–insertion		De novo	–
CNV	409	F	MPSI	2	*SCN2A, SCN1A*	Microdeletion	Microdeletion	3,726	De novo	–

OS, Ohtahara syndrome; EME, early myoclonic encephalopathy; MAE, myoclonic astatic epilepsy; DS, Dravet syndrome; WS, West syndrome; PCH, pontocerebellar hypoplasia; MPSI, malignant migrating partial seizures in infancy; SNVs, single nucleotide variants; CNVs, copy number variations; EOEEs, early onset epileptic encephalopathies.

mutation. Of these 12 mutations, 9 were single-nucleotide variants (2 nonsense, 3 splice-site, and 4 missense mutations) and two were small indels leading to frameshifts. The other mutation was a microdeletion. All these 11 point mutations were confirmed by Sanger sequencing. Four of the mutations (*STXBP1* c.902+1G>A, *SCN1A* c.580G>A, *SCN1A* c.3714A>C, and *CDKL5* c.533G>A) have been reported in individuals with EOEEs, so are recurrent (Mancardi et al., 2006; Harkin et al., 2007; Azmanov et al., 2010; Liang et al., 2011; Milh et al., 2011). Nine of the 11 mutations occurred de novo. The other two could not be tested because the paternal sample for one patient (*SCN1A* c.580G>A) and parental samples for another patient (*SCN1A* c.3714A>C) were unavailable.

CNV analysis of the 53 patients revealed a microdeletion involving *SCN1A* and *SCN2A* at 2q24.3 in patient 409 (Fig. 2A). To investigate this mutation further, we performed genomic microarray analysis and identified an approximately 3.7-Mb microdeletion (Fig. 2B). The deletion contained 13 RefSeq genes including *SCN2A* and *SCN1A*. Breakpoint-specific PCR analysis of the patient and her parents confirmed that the rearrangement occurred de novo (Fig. 2C). The sequence of the junction fragment confirmed a 3,726,029-bp deletion (chr2: 164,420,771–168,146,801) (Fig. 2D).

Discussion

Several bench-top high-throughput sequencing platforms are now available (Glenn, 2011; Loman et al., 2012; Quail et al., 2012). We selected Illumina MiSeq because it provides reasonable sequence throughput (1.6 Gb per run), a low error rate, a short run time (27 h), and sufficiently long reads (150 bp). We captured genomic DNA fragments of target genes by 3× tiling complementary RNA oligonucleotide probes (Nord et al., 2011) and sequenced 24 samples per MiSeq run, achieving sufficient coverage (a mean read depth of 255) over the target regions. This high coverage enabled us to detect point mutations and CNVs simultaneously, and long reads enabled us to detect small indels (Krawitz et al., 2010). Mapping by Novoalign, we were able to detect indels ranging in size from a 10-bp deletion to a 9-bp duplication.

By evaluating depth of coverage ratios (Nord et al., 2011), we detected six control microdeletions and one novel microdeletion, ranging in size from 4.6 kb to 3.7 Mb. To date, CNVs causing EOEEs have been analyzed by array CGH and MLPA (Mulley & Mefford, 2011). Array CGH can detect genome-wide CNVs, but its standard resolution is relatively low (>10 kb). On the other hand, MLPA can detect CNVs in specific genes, including single exon deletions; however, it is difficult to screen many genes at a time because MLPA is limited to 50 target exons per reaction (Stuppia et al., 2012). In addition, copy number analysis using MLPA can be affected by single nucleotide variants and indels in regions corresponding to the MLPA probes (Stuppia et al., 2012). In contrast, targeted capture and sequencing can analyze all targeted genes to detect mutations and CNVs simultaneously. CNVs as small as a single exon can be identified. Because all the procedures—from